Entanglement Rate for Gaussian Continuous Variable Beams

Zhi Jiao Deng,[1,2] Steven J. M. Habraken,[1] and Florian Marquardt[1,3,*]

[1] *Institut für Theoretische Physik II, Friedrich-Alexander-Universität Erlangen-Nürnberg, Staudtstr. 7, D-91058 Erlangen, Germany*

[2] *Department of Physics, College of Science, National University of Defense Technology, Changsha 410073, People's Republic of China*

[3] *Max Planck Institute for the Science of Light, Günther-Scharowsky-Straße 1/Bau 24, D-91058 Erlangen, Germany*

We derive a general expression that quantifies the total entanglement production rate in continuous variable systems, where a source emits two entangled Gaussian beams with arbitrary correlators. This expression is especially useful for situations where the source emits an arbitrary frequency spectrum, e.g. when cavities are involved. To exemplify its meaning and potential, we apply it to a four-mode optomechanical setup that enables the simultaneous up- and down-conversion of photons from a drive laser into entangled photon pairs. This setup is efficient in that both the drive and the optomechanical up- and down-conversion can be fully resonant.

PACS numbers: 03.67.Mn, 42.50.Dv, 42.50.Wk, 07.10.Cm

arXiv:1406.7815v2 [quant-ph] 1 Mar 2016

* Florian.Marquardt@physik.uni-erlangen.de

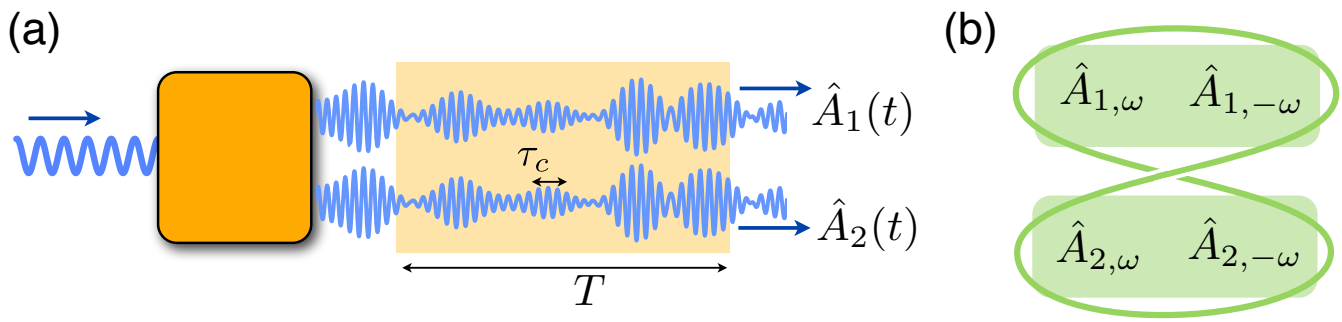

Figure 1. (a) A source of two entangled beams, where the aim is to calculate the entanglement between beams 1 and 2 in the large time interval T. (b) Frequency modes that are correlated (entangled) in the limit of large T.

I. INTRODUCTION

Entanglement is an essential feature of quantum mechanics and a crucial resource for quantum communication and information processing. The most common situation involves a source that continuously produces entangled beams. One of the most natural characteristics of such a source is obviously the rate at which it generates entanglement. If the source sends out pairs of entangled particles, with subsequent pairs completely independent, this rate can simply be defined as the entanglement of each pair, divided by the time between pairs. However, such a naive approach fails if there are correlations between subsequent pairs, or if we consider entangled beams of radiation that cannot be naturally decomposed into well-defined pairs of particles. In particular, this is true for the very important case of continuous variable (CV) entangled beams. Although many quantum information protocols exploit qubits, with their discrete state space, the original Einstein-Podolsky-Rosen [1] entanglement involves continuous variables, and CV entanglement has many modern applications [2–8].

In this article, we set out to provide a general definition for an entanglement rate in such nontrivial situations. It will turn out that our general definition, when applied to stationary Gaussian CV beams, gives rise to a frequency integral over what we call a "spectral density of entanglement". We show how to obtain this from the two-point time correlators of the entangled beams, using a suitable additive entanglement measure (the logarithmic negativity [9]). For one of the most common situations, we also provide explicit analytical expressions. Our definition of the entanglement rate is particularly important for setups where the output spectrum is arbitrary (e.g. containing one or several peaks). This is a widespread case, since the generation of CV-entangled radiation beams is often enhanced by using cavity modes (e.g. [10, 11] in the microwave domain, or [12, 13] in the optical domain). Recently, the authors of the first experiment on spatially separated CV entanglement in superconducting circuits even quantified their source by quoting the effective number of entangled bits per second [10], estimated from the bandwidth of the circuit and the entanglement between two modes. Our entanglement rate would provide a precisely defined way to quantitatively characterize such situations.

After we introduce and discuss the general definition, we illustrate our entanglement rate by applying it to a four-mode optomechanical setup that allows the fully resonant, and thereby efficient, generation of entanglement. The rapidly developing field of cavity optomechanics focuses on the dynamics of photons and phonons coupled via radiation forces, see [14] for a recent review. The optomechanical interaction has been predicted to produce entanglement, e.g. between optics and mechanics [15–20] or between light modes [21–31]. Recently, optomechanical entanglement was demonstrated experimentally for the first time, in a microwave circuit [32], making its analysis especially timely.

II. THE ENTANGLEMENT RATE

The situation we have in mind is very general: A source emits two CV-entangled beams, described by bosonic fields $\hat{A}_1(t)$ and $\hat{A}_2(t)$, see Fig. 1a. These could be, for example, two light beams of different polarization or fields propagating along two different waveguides. Typical sources might be a nonlinear crystal optical resonator driven by a pump beam, a driven optomechanical cavity, or a driven on-chip microwave cavity containing nonlinear elements like Josephson junctions.

We focus on the important regime of generating stationary Gaussian CV-entanglement. In that regime, one treats the pump as classical and then obtains a quadratic Hamiltonian, leading to Gaussian statistics of the emitted beams. Because of the pump, that Hamiltonian will be time-dependent, containing terms of the form $\hat{a}_c^\dagger \hat{a}_c^\dagger e^{-i\omega_p t} + h.c.$, where

$\hat{a}_c$ would be a cavity mode (our analysis also applies for several different modes). Here ω_p is the pump frequency if the original nonlinearity was of the $\chi^{(2)}$-type, $\hat{a}_c^\dagger \hat{a}_c^\dagger \hat{a}_p + \text{h.c.}$, whereas ω_p would be twice the pump frequency for a $\chi^{(3)}$-type nonlinearity $\hat{a}_c^\dagger \hat{a}_c^\dagger \hat{a}_p^2$. As is usual in such situations, it will be most useful to switch to a frame rotating at the frequency $\omega_p/2$, such that the Hamiltonian becomes time-independent and we are dealing with a stationary problem. In that new frame, $\omega = 0$ relates to the pump frequency.

Our analysis then focusses on the entanglement properties of the fields $\hat{A}_{1,2}(t)$ emitted from any such source. Being Gaussian, these fields are completely characterized by their two-time correlators. The details of the source do not matter, except that it is assumed to produce Gaussian beams that are stationary, i.e. where the correlators only depend on the time-difference.

At this point we note that in some situations it may also be natural to consider only a single field $\hat{A}(t)$, propagating along a single waveguide. Then, frequency components centered symmetrically around the pump frequency can be entangled, and they may afterwards be directed to two different output ports by frequency-filtering. For such a situation, we can still apply our approach if we define $\hat{A}_1(t)$ to contain the positive frequency ($\omega > 0$) components of the field $\hat{A}(t)$, while likewise $\hat{A}_2(t)$ would contain the negative frequency ($\omega < 0$) components, where ω is already determined with respect to the rotating frame.

Since the situation is stationary, it is natural to try and define an *entanglement rate*, i.e. the entanglement per unit time emitted from the source. We propose to do this in the most natural way by calculating the *overall* amount of entanglement between the two beams in a long time interval T and then dividing by T, in the end sending T to infinity:

$$\Gamma_E \equiv \lim_{T\to\infty} \frac{E(T)}{T} \,. \tag{1}$$

This definition is not constrained to CV entangled beams or to Gaussian states. It only requires (a) stationarity of the source, (b) an entanglement measure that is additive for product states, and (c) a finite correlation time τ_c for the beams. Given such a finite correlation time, the fields on two subsequent time-intervals of length $T \gg \tau_c$ are not correlated to a very good approximation. This holds because even though there may be remaining correlations near the boundary between the time-intervals, these are appreciable only up to a distance of order τ_c from the boundary and can be neglected in the limit $T \gg \tau_c$. Due to the additivity (and stationarity), we then get $E(2T) \approx 2E(T)$, such that the entanglement rate calculated for time intervals of sizes T or $2T$ is the same (up to the small corrections which we can neglect in the limit of large T).

From now on, we specialize to stationary Gaussian CV entangled beams. We will use the logarithmic negativity [4, 9] E_N as an entanglement measure, since it is both straightforwardly evaluated for Gaussian multi-mode states and has the important property of additivity.

Let us now consider the fields $\hat{A}_s(t)$ on the interval $[0, T]$, even though they are defined for all times t. We can define discrete frequency modes ($s = 1, 2$):

$$\hat{A}_s(t) = \frac{1}{\sqrt{T}} \sum_{\omega = j2\pi/T} \hat{A}_{s,\omega} e^{-i\omega t} \,. \tag{2}$$

The normalization is chosen such that the $\hat{A}_{s,\omega}$ fulfill bosonic commutation relations, $\left[\hat{A}_{s,\omega}, \hat{A}^\dagger_{s',\omega'}\right] = \delta_{s,s'}\delta_{\omega,\omega'}$, where $\omega = j2\pi/T$ is discrete, with j an integer.

We now want to calculate the full logarithmic negativity $E_N(T)$ between the two beams on that time interval, which is equivalent to the entanglement between two sets of harmonic oscillators [33]. In our case, we are even considering infinitely many harmonic oscillators $\hat{A}_{s,\omega}$. We stress that the entanglement $E_N(T)$ is (of course) independent of our choice of basis for each of the beams, as a different choice of basis amounts to implementing a local unitary transformation. The correlations between the two beams can be arbitrary, except that they are supposed to decay beyond some correlation time τ_c (which is true in any reasonable physical situation). As already mentioned above, we will assume that $T \gg \tau_c$, such that the correlations between subsequent intervals of size T can be neglected. In that limit, we can use stationarity to show that only the following types of correlators may be nonzero in the present situation, up to corrections that are small in τ_c/T: $\left\langle \hat{A}^\dagger_{s,\omega} \hat{A}_{s',\omega} \right\rangle$ and $\left\langle \hat{A}_{s,\omega} \hat{A}_{s',-\omega} \right\rangle$ (and their conjugates). For example, we find

$$\left\langle \hat{A}^\dagger_{s,\omega} \hat{A}_{s',\omega'} \right\rangle \approx \delta_{\omega,\omega'} \left\langle \hat{A}^\dagger_s \hat{A}_{s'} \right\rangle_{-\omega} \,, \tag{3}$$

where we have defined the Fourier transform of the correlator: $\left\langle \hat{A}\hat{B} \right\rangle_\omega \equiv \int_{-\infty}^{+\infty} dt\, e^{i\omega t} \left\langle \hat{A}(t)\hat{B}(0) \right\rangle$. Likewise, we have $\left\langle \hat{A}_{s,\omega}\hat{A}_{s',\omega'} \right\rangle = \delta_{\omega,-\omega'} \left\langle \hat{A}_s\hat{A}_{s'} \right\rangle_\omega$.

In summary, for any given $\omega > 0$, only the correlators involving the modes ω and $-\omega$ are nonzero (see Fig. 1b). There is entanglement $E_N[\omega]$ between the two modes $\hat{A}_{1,\omega}$ and $\hat{A}_{1,-\omega}$ of beam 1 with the two modes $\hat{A}_{2,\omega}$ and $\hat{A}_{2,-\omega}$ of beam 2. Further below, we will show how $E_N[\omega]$ can be calculated from the correlators. The overall entanglement $E_N(T)$ between the two beams can then be decomposed into a sum, because of the additivity of the logarithmic negativity:

$$E_N(T) = \sum_{\omega>0} E_N[\omega]\,. \tag{4}$$

We note that $E_N[\omega]$ in the sum does not depend on T (after adopting the approximation of Eq. 3), although the number of summation terms does scale with T due to the discretization of ω.

The sum over discrete frequencies can be converted into an integral. To leading order at large T, we have $\sum_{\omega>0} E_N[\omega] \approx (2\pi/T)^{-1} \int_0^\infty d\omega\, E_N[\omega]$. Therefore, we can identify $E_N[\omega]$ as the *"spectral density of entanglement"* [34]. In addition, this confirms that the total entanglement indeed grows linearly in T for sufficiently large times. As a consequence we finally obtain the *entanglement rate*:

$$\Gamma_E \equiv \lim_{T\to\infty} \frac{E_N(T)}{T} = \int_0^\infty \frac{d\omega}{2\pi} E_N[\omega]\,. \tag{5}$$

This shows that $E_N[\omega]$ itself may be interpreted as the *entanglement rate per frequency interval*. It is possible to give an explicit expression for $E_N[\omega]$ in terms of the covariance matrix containing the correlators [9]. The general case, involving the four modes $\hat{A}_{1,\omega}$, $\hat{A}_{1,-\omega}$, $\hat{A}_{2,\omega}$, and $\hat{A}_{2,-\omega}$, is a bit cumbersome, requiring the symplectic diagonalization of a 8×8 covariance matrix. However, the expressions simplify considerably if there is purely two-mode squeezing, i.e. if the intra-mode correlators $\left\langle \hat{A}_{s,\omega}\hat{A}_{s,-\omega} \right\rangle$ vanish. In that case, we find

$$E_N[\omega] = E[\omega] + E[-\omega]\,. \tag{6}$$

For positive ω, $E[\omega]$ is the entanglement between $\hat{A}_{1,\omega}$ and $\hat{A}_{2,-\omega}$ while $E[-\omega]$ is the entanglement between $\hat{A}_{1,-\omega}$ and $\hat{A}_{2,\omega}$. In contrast to $E_N[\omega]$, the density $E[\omega]$ is double-sided (has contributions both at negative and positive frequencies). We note that in the following we will also commonly refer to $E[\omega]$ as the spectral density of entanglement, since it is closely related to $E_N[\omega]$. Setting $n_+ \equiv \left\langle \hat{A}^\dagger_{1,\omega}\hat{A}_{1,\omega} \right\rangle + \frac{1}{2}$, $n_- \equiv \left\langle \hat{A}^\dagger_{2,-\omega}\hat{A}_{2,-\omega} \right\rangle + \frac{1}{2}$, and $\xi \equiv \left\langle \hat{A}_{1,\omega}\hat{A}_{2,-\omega} \right\rangle$, we have:

$$E[\omega] = \max(0, -\ln(2\eta_-)), \tag{7}$$

$$2\eta_- = n_+ + n_- - \sqrt{(n_+ - n_-)^2 + 4\,|\xi|^2}\,. \tag{8}$$

As an aside we note that we choose to work with the natural logarithm in our discussion (some articles use $\log_2$, which is more natural for discrete qubits [9]).

In this special case, the entanglement rate is therefore:

$$\Gamma_E = \int_{-\infty}^{+\infty} \frac{d\omega}{2\pi} E[\omega]\,. \tag{9}$$

III. RELATION TO ENTANGLEMENT BETWEEN WAVE PACKETS

We now want to connect our general result to previously applied approaches for quantifying the entanglement in such situations. It is a common procedure to employ normalized mode functions ("filter functions") $f_s(t)$ that have the shape of wave packets, in order to define two harmonic oscillator modes, one for each beam:

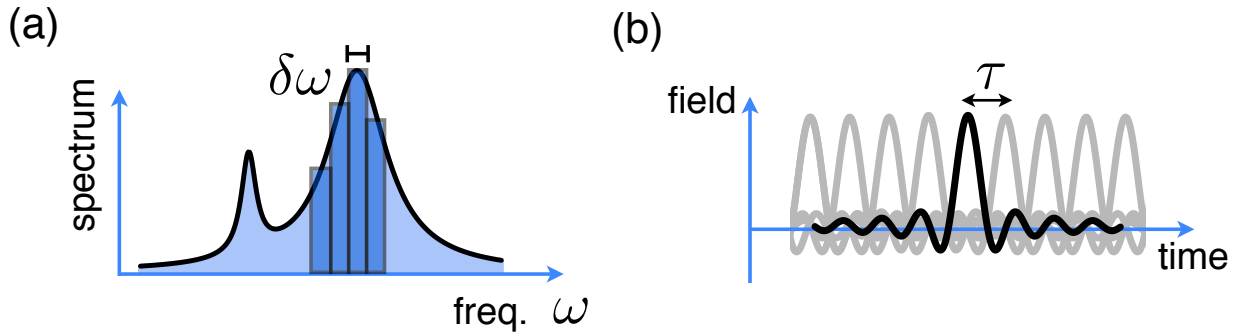

Figure 2. Wave packet picture that can be used in understanding the entanglement rate. (a) For each of the beams, we imagine to frequency-filter the field, with a filter size $\delta\omega$. (b) In time-space, this corresponds to wave packets spaced by $\tau = 2\pi/\delta\omega$. These form a complete basis on a time-frequency grid. The use of a wave packet basis on a time-frequency grid in the context of quantum noise is reviewd in [35].

$$\hat{a}_s \equiv \int_{-\infty}^{+\infty} dt\, f_s(t)\hat{A}_s(t)\,. \tag{10}$$

Here $\int_{-\infty}^{+\infty} |f_s(t)|^2\, dt = 1$. The entanglement between $\hat{a}_1$ and $\hat{a}_2$ can then be calculated, e.g. again using the logarithmic negativity as an entanglement measure. This filtering analysis has been applied to several settings [21, 26, 31], for a detailed explanation see e.g. [21, 22]. The catch is that this procedure introduces a filtering time τ (the extent of the wave packets), and the results will be a function of τ, which is usually taken to be arbitrary.

How would one loosely define an entanglement rate based on this procedure? We can imagine that there is a stream of such wave packets, with a spacing of about τ (where care would have to be taken to define them to be orthogonal). A simple, though phenomenological approach to define an entanglement rate would be to simply calculate the ratio E_N^τ/τ.

However, it is clear that this approach is not systematic. In fact, it cannot always cover the full entanglement, since there may be entanglement in components of the beam that are orthogonal to the filter functions which are employed. In addition, there is some arbitrariness in the choice of filter function (and, thus, even in the definition of τ). Moreover, one may have situations where there are temporal correlations extending beyond τ. Then, the entanglement present in the beams may be underestimated. If one tries to remedy this problem by choosing larger τ, then the filter bandwidth shrinks and one may miss entanglement present at other frequencies.

It turns out that an approach based on wave packets can be made to work, but only if one constructs a suitable complete basis that has a clear physical meaning. It is more systematic than the naive filtering approach described so far and it covers all the entanglement. In addition, it can be related to a direct physical prescription, and we will see that it leads to the same results as our general, basis-independent definition discussed in the previous section.

For simplicity, focus on the situation with only cross-correlations (no intra-beam squeezing) that we discussed at the end of section II. Imagine one sends one beam through a frequency filter $[\omega, \omega + \delta\omega]$, where $\delta\omega = 2\pi/\tau$. Likewise, the other beam will be sent through another filter, at negative frequencies $[-\omega, -\omega - \delta\omega]$. Now construct a complete set of orthogonal wave packet modes ("Wannier basis") with a spacing τ in time, which are able to fully represent the filtered beams (see Fig. 2). As we show in the appendix V A, the logarithmic negativity E_N^τ between two such wave packet modes (one in each beam, at equal time-slots) is related to $E[\omega]$ in the limit $\tau \gg \tau_c$:

$$\lim_{\tau\to\infty} E_N^\tau = E[\omega]\,. \tag{11}$$

As a consequence, the general definition of the previous section agrees with the entanglement rate calculated from such a wave packet picture. This wave packet approach can also be viewed as representing the following physical procedure: Split each of the two entangled beams into many frequency-filtered output beams, where the frequency resolution $\delta\omega = 2\pi/\tau$ has been chosen fine enough, such that $\delta\omega \ll 1/\tau_c$. The rate Γ_E quantifies the total entanglement per unit time contained in the sum of those streams (since it was defined that way in the previous section). Each pair of wave packets (of length τ) can in principle be exploited for an application such as CV quantum teleportation. A concrete physical measurement of the entanglement between any two wave packets could be performed in a standard

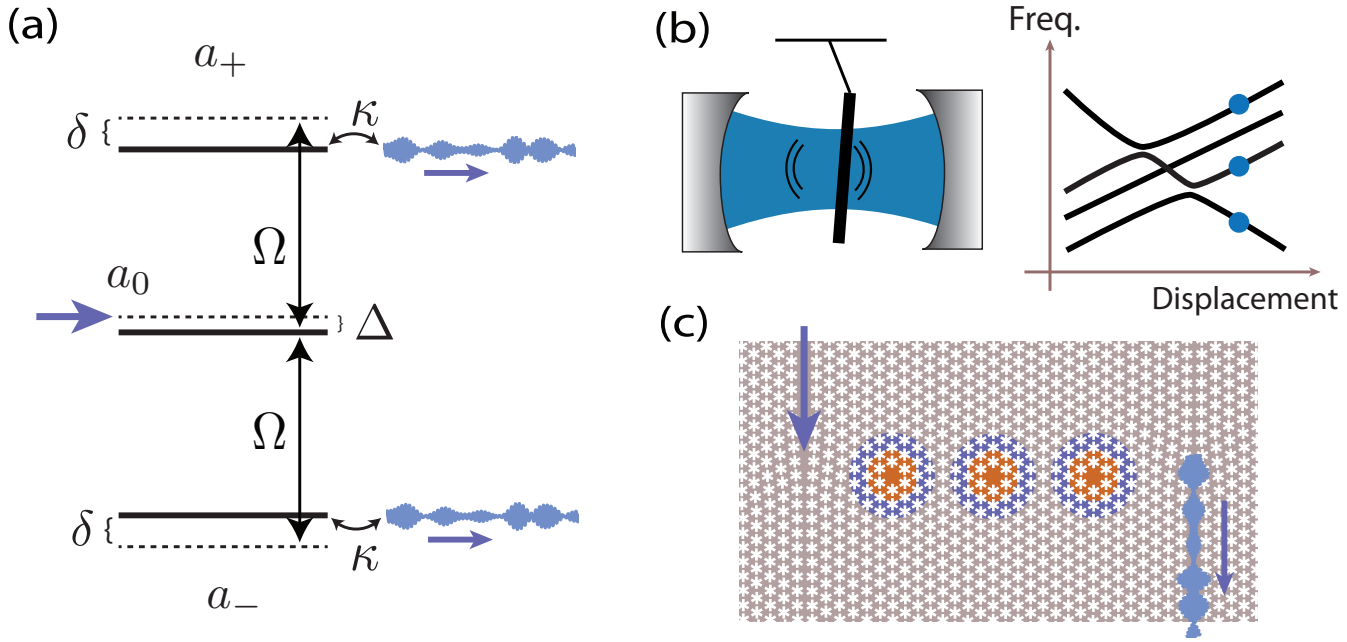

Figure 3. (a) Level diagram: the optical level distance almost matches the vibrational frequency Ω so that phonon-mediated transitions between the optical levels occur. (b) Schematic for a possible implementation in a membrane-in-the-middle setup; three of the optical modes constitute an equidistant triplet for a suitable membrane position and tilt angle. (c) Schematic for the possible implementation in an optomechanical crystal, with one incoupling and one outcoupling waveguide.

way, using homodyne measurements. For example, the local oscillator can provide strong pulses that are shaped in the form of the wave packet modes that we want to consider.

IV. A SPECIFIC OPTOMECHANICAL EXAMPLE, AND ITS IMPLEMENTATION

A. Model

We illustrate the features of the entanglement rate in a model describing the effective interaction between two localized optical modes ($\hat{a}_+$ and $\hat{a}_-$) and a mechanical mode ($\hat{b}$):

$$\begin{aligned}\hat{H}/\hbar = &-\Delta(\hat{a}_+^\dagger\hat{a}_+ + \hat{a}_-^\dagger\hat{a}_-) + \delta\hat{b}^\dagger\hat{b} \\ &-\frac{g}{2}\{(\hat{a}_+ + \hat{a}_-^\dagger)\hat{b}^\dagger + (a_+^\dagger + \hat{a}_-)\hat{b}\}\ ,\end{aligned} \tag{12}$$

Similar Hamiltonians have been studied previously in the context of entanglement generation between light modes [21–31]. For instance, Wang and Clerk [28] studied intra-cavity entanglement, while Tian [29] investigated also the stationary output entanglement. We note that, more recently, an analysis of the output entanglement in the setup with $\Delta = \delta = 0$ (but with unequal couplings for up- and down-conversion) was provided in [30].

Before proceeding, we note how to implement this model using three equidistant optical modes, enhancing the efficiency beyond previous suggestions. The optical mode spacing J is nearly resonant with the vibration frequency Ω, with a frequency mismatch $\delta = \Omega - J$ (Fig. 3a). A laser drives the center optical mode at ω_0, with a detuning $\Delta = \omega_L - \omega_0$. An optomechanical interaction of the kind $\hbar g_0 \hat{a}_+^\dagger \hat{a}_0(\hat{b} + \hat{b}^\dagger)$, and similarly for $\hat{a}_-$, scatters photons up and down, into modes $\hat{a}_+$ and $\hat{a}_-$, while simultaneously destroying (creating) phonons. When a phonon is virtually emitted and re-absorbed, an effective four-wave mixing process is induced, generating a pair of $\hat{a}_+$ and $\hat{a}_-$ photons out of a pair of $\hat{a}_0$ photons. Thus, two-mode vacuum squeezing (EPR entanglement) is produced. We assume that the drive is strong and we can replace $\hat{a}_0$ by the coherent amplitude $\alpha = \langle\hat{a}_0\rangle$. This yields the Hamiltonian (12) with $g \equiv 2g_0\alpha$, provided we choose frames rotating at $\omega_L \pm J$ for the modes $\hat{a}_\pm$, and at J for $\hat{b}$. Moreover, only nearly resonant terms are kept, which is allowed if $J, \Omega \gg g, \kappa$, where κ is the optical intensity decay rate.

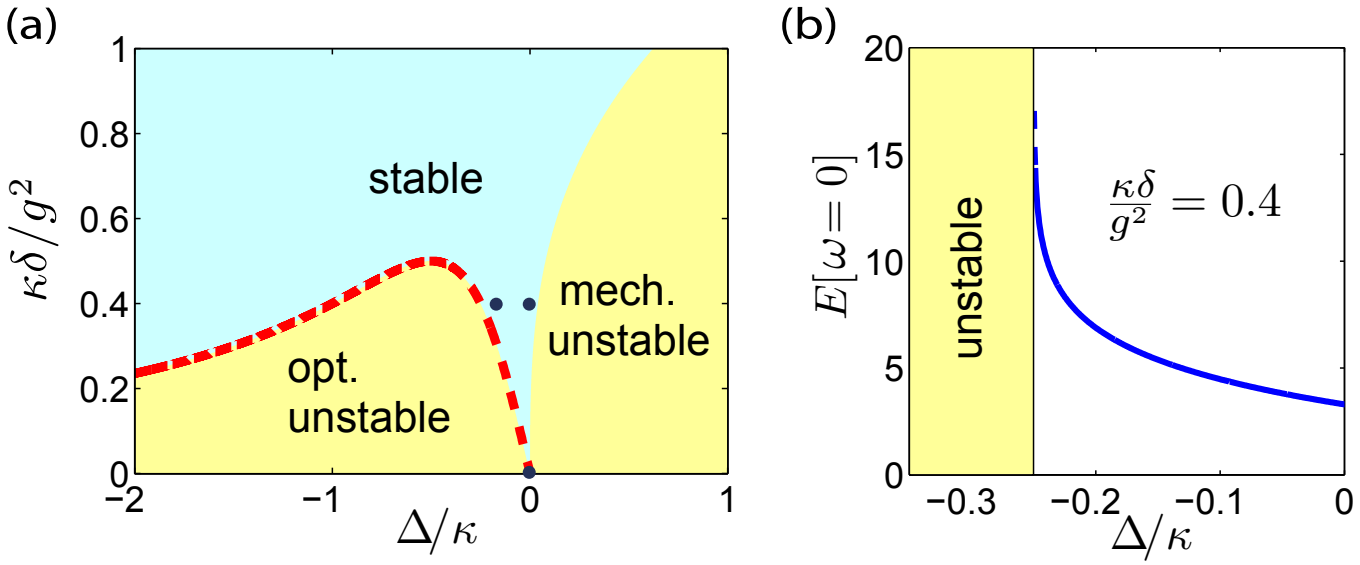

Figure 4. (a) Stability diagram of the model, vs. frequency mismatch δ and laser detuning Δ, for $g/\kappa = 5$ and $\Gamma/\kappa = 10^{-3}$. Stability boundary in the effective optical model: red dashed line. Parameter values corresponding to the (stable) blue points will be studied below. (b) Diverging entanglement from the effective optical model at the boundary of stability.

Possible experimental implementations include a membrane-in-the-middle setup tuned to a point with three equidistant modes [36–38] (Fig. 3b) or coupled optomechanical cells, e.g. in an optomechanical crystal [39, 40] (Fig. 3c), see the appendix. Such a triply-resonant setup enhances the efficiency: As compared to previous suggestions with only one resonantly driven mode, generating entangled Stokes and anti-Stokes sidebands (similar to [21]), one wins a factor $\Omega^4/(\delta^2+(\kappa/2)^2)^2 \gg 1$ in the intensity of the entangled output beams, while compared to setups with two optical ouput modes (e.g. [28, 29]), one wins a factor $(2\Omega/\kappa)^4 \gg 1$, for fixed input laser power and $\Delta = 0$.

We use standard input-output theory[41] for our analysis:

$$\begin{aligned}\dot{\hat{a}}_j &= \frac{i}{\hbar}[\hat{H},\hat{a}_j] - \frac{\kappa}{2}\hat{a}_j - \sqrt{\kappa}\hat{a}_{j,\mathrm{in}}(t),\\ \dot{\hat{b}} &= \frac{i}{\hbar}[\hat{H},\hat{b}] - \frac{\Gamma}{2}\hat{b} - \sqrt{\Gamma}\hat{b}_{\mathrm{in}}(t)\end{aligned} \tag{13}$$

Here Γ is the mechanical damping rate and $j = \pm$. As usual, $\langle\hat{b}^\dagger_{\mathrm{in}}(t)\hat{b}_{\mathrm{in}}(0)\rangle = n_{\mathrm{th}}\delta(t)$ and $\langle\hat{b}_{\mathrm{in}}(t)\hat{b}^\dagger_{\mathrm{in}}(0)\rangle = (n_{\mathrm{th}}+1)\delta(t)$, with $n_{\mathrm{th}} = (\exp(\hbar\Omega/(k_{\mathrm{B}}T))-1)^{-1}$ the thermal occupation, and likewise for $\hat{a}_{j,\mathrm{in}}$ (but without thermal noise). Solving Eqs. (13) and employing $\hat{a}_{j,\mathrm{out}}(t) = \hat{a}_{j,\mathrm{in}}(t) + \sqrt{\kappa}\hat{a}_j(t)$, we find the linear relation between output and input fields in terms of a scattering matrix.

Coming back to our general definition of the entanglement rate, we would consider $\hat{a}_{+,\mathrm{out}}(t)$ as the first beam $\hat{A}_1(t)$ and $\hat{a}_{-,\mathrm{out}}(t)$ as the second beam $\hat{A}_2(t)$. It is not difficult to show (and can be confirmed by direct calculation) that there is no intra-beam squeezing, i.e. $\left\langle \hat{A}_{1,\omega}\hat{A}_{1,-\omega}\right\rangle = 0$ and likewise for beam 2. Thus, we want to employ the formulas Eqs. (7) and (9) in order to find the contributions to the spectral density of entanglement and the entanglement rate.

To calculate $E[\omega]$, we need the correlators of the two beams. Entangled photon pairs are emitted at *physical* frequencies $\omega_L \pm J \pm \omega$, corresponding to $\pm\omega$ in our rotating frame. We have to evaluate correlators like $\int_{-\infty}^{+\infty} e^{i\omega t}\langle\hat{a}_{+,\mathrm{out}}(t)\hat{a}_{-,\mathrm{out}}(0)\rangle\, dt$ as shown in appendix V E.

B. Results

We first address some general features. The system can become unstable (Fig. 4a), both towards mechanical and optical oscillations. The optical stability boundary is approximately given by $(\Delta+g^2/2\delta)\Delta+(\kappa/2)^2 = 0$. Eliminating

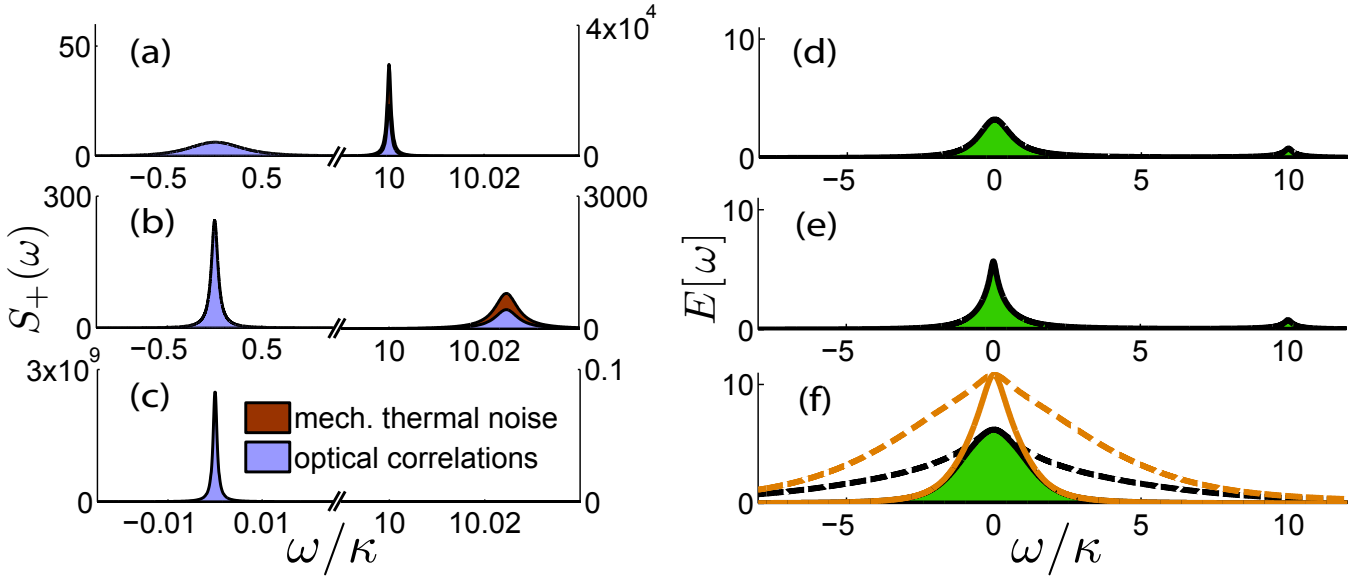

Figure 5. The output spectrum $S_+(\omega)$ for the beam from the upper optical mode, plotted for three typical situations (a,b,c) at a fixed temperature ($n_{\rm th} = 50$), with $g/\kappa = 5$ and $\Gamma/\kappa = 10^{-3}$. Blue vs. brown distinguish optical vs. mechanical noise contributions. (a) resonant drive, off-resonant mechanical mode ($\Delta = 0$, $\delta = 10\kappa$); (b) near the optical instability ($\Delta = -0.2\kappa$, $\delta = 10\kappa$); (c) doubly resonant ($\Delta = \delta = 0$). Note the differences in vertical and horizontal scales for the peaks. (d,e,f) The spectral density of entanglement $E[\omega]$, corresponding to (a,b,c). Additional curves in (f) correspond to $\Gamma/\kappa = 5 \cdot 10^{-2}$(dashed) and $\Gamma/\kappa = 10^{-3}$ (solid), for $n_{\rm th} = 0$ (orange) and $n_{\rm th} = 50$ (black), at fixed cooperativity $\mathcal{C} = g^2/\kappa\Gamma = 2.5 \cdot 10^4$.

the mechanical mode (for $\delta \gg \kappa$, Γ, g, $|\Delta|$), we obtain an effective optical model, which yields the photon pair creation rate $\Gamma_{\rm pairs} = \left(\frac{g^2}{4\delta}\right)^2 \frac{\kappa}{2}[(\kappa/2)^2 + (\triangle + \frac{g^2}{2\delta})\triangle]^{-1}$. This diverges at the optical stability boundary.

We now focus on the spectral density of entanglement $E[\omega]$ that characterizes the output beams, and especially the entanglement rate. In contrast to the intra-cavity entanglement (discussed in [28, 29]), we find that $E[\omega]$ is not bounded. This is similar to the difference between intra-cavity and output squeezing [42–44]. Numerical plots of $E[\omega]$ for the Hamiltonian (12) have been shown so far [29] only for the special case $\Delta = \delta = 0$ and asymmetric optomechanical couplings. Entanglement of temporal modes was also discussed for a pulsed scheme [31] in the case $\delta \neq 0$.

The output entanglement grows significantly at the stability boundary (Fig. 4b), even diverging in the effective optical model. This is typical near an instability but it comes at the price of linewidth narrowing, reducing the entanglement rate.

In order to appreciate this, we now discuss the output intensity spectrum, $S_+(\omega) = \int e^{-i\omega t} \left\langle \hat{a}^\dagger_{+,\rm out}(t)\hat{a}_{+,\rm out}(0)\right\rangle dt$, in Fig. 5a,b,c. We expect that any mechanical noise contributing to the optical output is deleterious for entanglement, which is confirmed by explicit calculation. Thus, we plot the spectrum in an instructive way, distinguishing optical and mechanical contributions, as obtained from the linear relation $\hat{a}_{+,\rm out}(\omega) = \ldots \hat{a}_{+,\rm in}(\omega) + \ldots (\hat{a}^\dagger_{-,\rm in})(\omega) + \ldots \hat{b}_{\rm in}(\omega)$. There are typically two peaks, separated by $\delta = \Omega - J$ and containing primarily optical or mechanical noise, respectively. Near the optical instability (Fig. 5b), the optical peak gets strong and narrow.

When the optical mode spacing matches the mechanical frequency ($\delta = 0$) and the laser is on resonance ($\Delta = 0$), the two peaks merge and have a narrow linewidth set by the mechanical damping rate Γ (Fig. 5c). It will turn out that the entanglement rate is maximized near this point. This is entirely counterintuitive: One might expect that at $\delta = 0$ mechanical noise is injected into the output beams, destroying entanglement. However, we find that the optical noise can completely overwhelm the mechanical noise for strong driving, when the cooperativity is sufficiently large, $\mathcal{C} \equiv g^2/\kappa\Gamma \gg n_{\rm th}$.

The spectral density $E[\omega]$ is shown in Fig. 5d,e,f. Typically, $E[\omega]$ is maximal at the optical peak near $\omega = 0$. For the important case $\Delta = \delta = 0$, we find an analytical expression, $E[\omega = 0] = -\ln(2\eta_-)$, where

$$\eta_- = 4\mathcal{C}(\mathcal{C} + n_{\rm th} + \frac{1}{2}) + \frac{1}{2} - 2\mathcal{C}\sqrt{1 + 4(\mathcal{C} + n_{\rm th} + \frac{1}{2})^2} \tag{14}$$

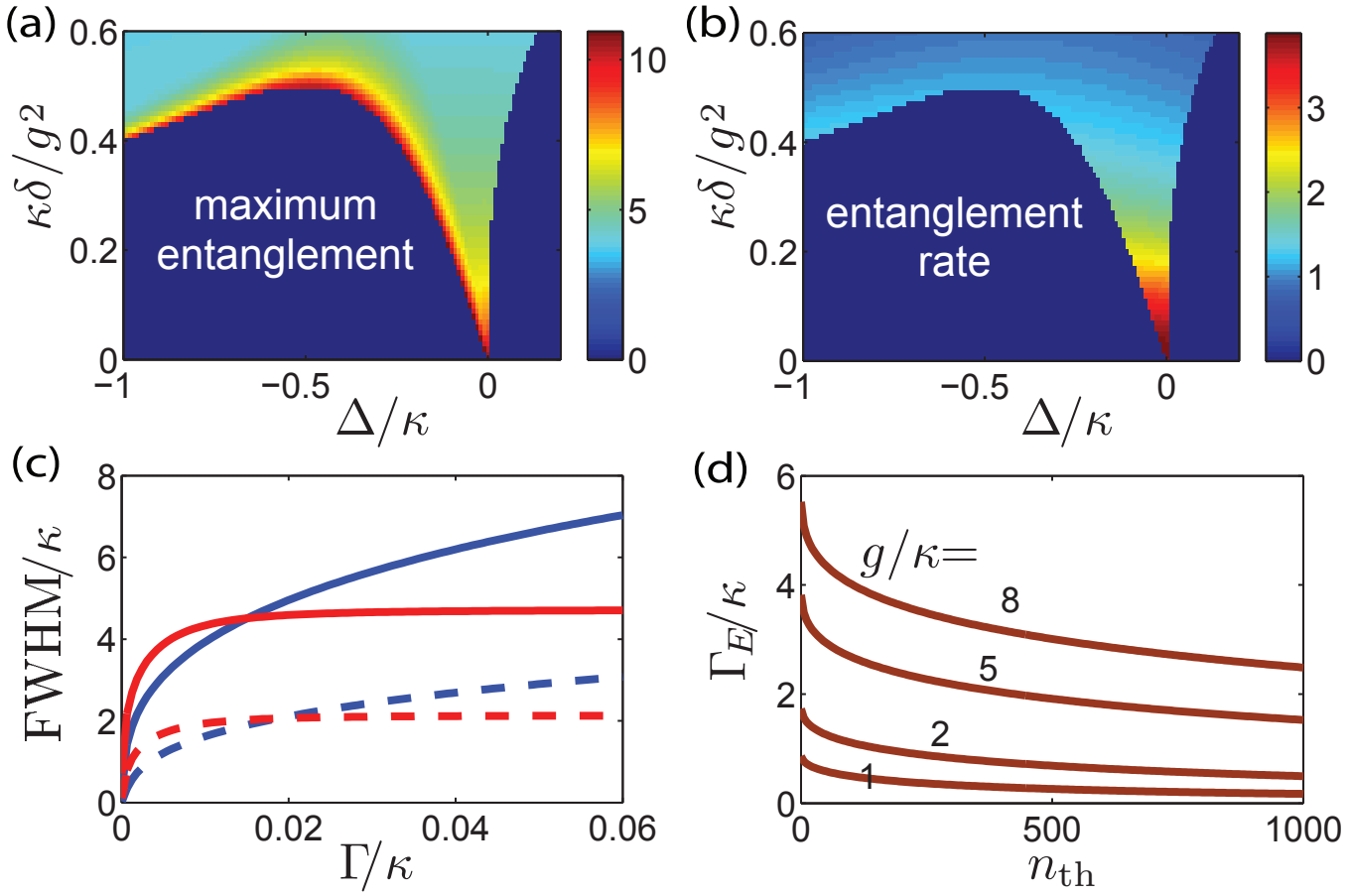

Figure 6. (a) Spectral density of entanglement, maximized over frequency, $\max_\omega E[\omega]$, and (b) total entanglement rate $\Gamma_E = \int E[\omega]d\omega/2\pi$ (in units of κ), both shown as a function of frequency mismatch δ and laser detuning Δ, for $n_{\rm th} = 0$, $g/\kappa = 5$ and $\Gamma/\kappa = 10^{-3}$. (c) The full-width-half-maximum (FWHM) of the peak in $E[\omega]$ as a function of Γ/κ, for fixed cooperativity $\mathcal{C} = 2.5 \cdot 10^4$ (solid) and $\mathcal{C} = 10^3$ (dashed), at $\delta = \Delta = 0$. (Blue: $n_{\rm th} = 0$, Red : $n_{\rm th} = 50$). (d) Temperature dependence of Γ_E ($\delta = \Delta = 0$ and $\Gamma/\kappa = 10^{-3}$).

depends on both driving (via $\mathcal{C}$) and temperature. We checked that choosing different optomechanical couplings for the two modes $\hat{a}_\pm$ will not increase $E[\omega = 0]$, in contrast to the intra-cavity case [28].

In Fig. 6a,b, we compare the maximum of the spectral density of entanglement, $E_{\rm max} \equiv \max_\omega E[\omega]$, and the entanglement rate $\Gamma_E = \int E[\omega]d\omega/2\pi$. While $E_{\rm max}$ becomes large near the optical boundary of stability, the entanglement rate there remains small, due to the narrow bandwidth. This will be a general feature in many similar systems. Rather, $\Gamma_{\rm E}$ is optimal near $\delta = \Delta = 0$. We found that, as the mechanical damping rate increases, the optimum shifts away from $\Delta = \delta = 0$.

The entanglement rate depends on the full shape of $E[\omega]$, in particular the peak width(s). Crucially, those widths are distinct from those in the output spectrum, due to the nonlinear (logarithmic) dependence of E on parameters. For example, in the case $\Delta = \delta = 0$ of greatest interest, the peak width (see Fig. 5f, Fig. 6c) is not set by the small mechanical linewidth Γ, unlike for the output spectrum discussed above. Thus, the values of the entanglement rate Γ_E for the parameters explored here are much larger, of the order $\kappa \cdot \max_\omega E[\omega]$. For increasing temperatures, $\Gamma_{\rm E}$ decreases, but only slowly, indicating robust entanglement in this setup: $\Gamma_E \propto {\rm n}_{\rm th}^{-1}$, with the prefactor set by the cooperativity $\mathcal{C}$ (Fig. 6d).

V. CONCLUSIONS

We have introduced an entanglement rate as a quantitative measure for the CV entanglement production per unit time in setups involving resonant modes. The definition is natural, in that it simply characterizes the total entanglement between two beams within a time-interval of size T, in the limit $T \to \infty$. In principle, it is also more

general than the Gaussian CV case studied in the present manuscript.

Moreover, we have studied an optomechanical setup with one mechanical and three optical modes that allows fully resonant production of optical entanglement. The spectral density of entanglement and the overall entanglement rate are optimized for different parameter choices. The concept introduced here should be useful for analyzing setups in other domains, like cavities with a Kerr medium [12, 13] or microwave resonators with nonlinearities [10, 11].

Acknowledgement. - We have benefited from discussions with A. Clerk, D. Vitali and T. Kiendl, as well as S. Kessler, A. Kronwald, R. Lauter, M. Ludwig, V. Peano, T. Paraiso, M. Schmidt and T. Weiss. ZJD thanks FM for his kind hospitality in Erlangen. This work was supported via an ERC Starting Grant OPTOMECH, via ITN cQOM, and via the DARPA program ORCHID. ZJD acknowledges support from the National Natural Science Foundation of China under Grants No. 11104353 and No. 11574398.

APPENDIX

A. Wave Packet Basis: General Scheme

In the main text, we claimed that our general entanglement rate can be connected to an approach of frequency-filtering and decomposing the filtered beams into wave packets. The natural way to make these notions precise is by using the Wannier-basis of wave packets $f_{m,n}(t)$ that live on a regular grid both in time, $t_n = n\tau$, and in frequency-space, $\omega_m = m\delta\omega$, where $\delta\omega = 2\pi/\tau$. The Fourier-transform $F_{m,n}(\omega) \equiv \int e^{i\omega t} f_{m,n}(t)dt/\sqrt{2\pi}$ of these wave packets is nonzero only in the interval $\omega \in [(m-\frac{1}{2})\delta\omega, (m+\frac{1}{2})\delta\omega)$, where $F_{m,n}(\omega) = \exp(i\omega t_n)/\sqrt{\delta\omega}$. The $F_{m,n}(\omega)$, and therefore also the $f_{m,n}(t)$, form an orthonormal basis. That makes it possible to decompose uniquely the output field into modes defined by these wave packets: $\hat{A}_s(t) = \sum_{m,n} \hat{a}^{(s)}_{m,n} f_{m,n}(t)$, where $\hat{a}^{(s)}_{m,n} = \int f^*_{m,n}(t)\hat{A}_s(t)\,dt$ annihilates a photon in mode (m,n), and $\left[\hat{a}^{(s)}_{m,n}, \hat{a}^{(s')\dagger}_{\tilde{m},\tilde{n}}\right] = \delta_{m,\tilde{m}}\delta_{n,\tilde{n}}\delta_{s,s'}$. In a typical application with a stationary-state source producing beams via parametric down-conversion or four-wave mixing, energy conservation dictates that pairs of frequencies ω_1 and ω_2 are entangled only when they obey $\omega_{\rm total} = \omega_1 + \omega_2$ (in the limit $\tau \to \infty$). In the rotating frame adopted in the main text, $\omega_{\rm total}$ would be zero.

We now calculate the logarithmic negativity E^τ_N between two wave packets of the two output fields, at the same time slot t_n and in suitable frequency slots ω and $-\omega$. For simplicity, we will assume a situation with purely inter-beam entanglement (no intra-beam squeezing), as discussed at the end of section II. A similar construction would apply to the more general case, even though then it would become necessary to consider the entanglement between two wave packets at ω and $-\omega$ of beam 1 with two wave packets at ω and $-\omega$ of beam 2.

To prepare for our definition of the entanglement rate, we have to discuss the dependence of E^τ_N on the filter time τ, especially for the limit $\tau \gg \tau_c$, where τ is much longer than the physical correlation time τ_c of the source (τ_c^{-1} is the width of the spectral peaks). First, this ensures that there will be no correlations between wave packets located at different time slots, such that we capture the full amount of entanglement. Second, we will now explain in this wave packet picture why E^τ_N tends to a well-defined limit for $\tau \to \infty$, which is consistent with direct calculations[21].

Consider enlarging the filter time τ by a factor M, shrinking the filter frequency interval by $\delta\omega' = \delta\omega/M$. In effect, the new wave packets of size $\tau' = M\tau$ encompass M of the old wave packets. That this coarse-graining keeps the correlators, and thus the entanglement E^τ_N, unchanged can be understood already from a very simple consideration. Take a suitably normalized sum of M operators, $\hat{X} = M^{-1/2}\sum_{n=1}^M \hat{X}_n$ and likewise $\hat{Y} = M^{-1/2}\sum_{n=1}^M \hat{Y}_n$. Then the correlator between these "averaged" operators will equal the original correlator: $\left\langle \hat{X}\hat{Y} \right\rangle = \left\langle \hat{X}_n\hat{Y}_n \right\rangle$. This holds provided there have been no cross-correlations and $\left\langle \hat{X}_n\hat{Y}_n \right\rangle$ is independent of n. The same logic applies to our case, where the new modes are properly normalized averages over the old modes: $\hat{a}^{'}_{m',n'} = \sum_n K_{m'}(n-n'M)\hat{a}_{m,n}$, with K encoding the overlap between the two basis sets. The detailed structure of K is not important for our argument, but essentially K is nonzero only in a range of size M, for $|n-n'M| \lesssim M$, and it is normalized: $\sum_n |K_{m'}(n-n'M)|^2 = 1$. As shown in the next section, this ensures a well-defined limit $E_N^{\tau\to\infty}$.

The entanglement rate for a given frequency slot m may now be defined naturally as $E^\tau_{N,m}/\tau$, the ratio between the entanglement $E^\tau_{N,m}$ contained in a pair of wave packets at that frequency and the time τ between those wave packets. (Here m would denote the index for beam 1 to which corresponds uniquely an index m_2 for beam 2, as explained above.) As the logarithmic negativity is additive, it makes sense to add up $E^\tau_{N,m}$ for all the small frequency intervals into which the emission of the source has been decomposed.

We have checked by direct calculation that $\lim_{\tau\to\infty} E^\tau_{N,m}$ defined here co-incides with the $E[\omega]$ defined in the main text (where $\omega = m\delta\omega$ is kept fixed in the limit $\tau \to \infty$, by adjusting m). This is despite the fact that $E^\tau_{N,m}$ is defined

with respect to Wannier basis modes, while $E[\omega]$ was defined from the Fourier components of the field on a finite time-interval of length $T \gg \tau_c$.

We thus have arrived again (in a different route), at the total entanglement rate:

$$\Gamma_E \equiv \lim_{\tau\to\infty} \sum_m \frac{E^{\tau}_{N,m}}{\tau} = \int_{-\infty}^{+\infty} \frac{d\omega}{2\pi} E[\omega]\,. \tag{15}$$

We have used $\delta\omega = 2\pi/\tau$ to convert the sum into an integral. In the limit $\tau \to \infty$, the details of the Wannier basis have become unimportant. $E[\omega]$ can now be calculated using any filter function.

B. More details on the Wannier basis

In this section, we present some more technical details on our wave packet based discussion of the entanglement rate. As defined in the main text and mentioned in the preceding section, we start from a complete orthonormal basis of packets that are localized both on a time-grid ($t_n = n\tau$) and a frequency-grid ($\omega_m = m\delta\omega$), where $\tau = 2\pi/\delta\omega$. In frequency space, these basis functions are defined as

$$F_{m,n}(\omega) = \frac{1}{\sqrt{\delta\omega}} e^{i\omega t_n}\,, \tag{16}$$

if $(m-1/2)\delta\omega \le \omega < (m+1/2)\delta\omega$, and $F_{m,n}(\omega) = 0$ otherwise. In time-space, this corresponds to the well-known Wannier-basis of sinc-shaped wave packets,

$$f_{m,n}(t) = \int F_{m,n}(\omega) e^{-i\omega t} \frac{d\omega}{\sqrt{2\pi}} = f_m(t - t_n)\,,$$

where

$$f_m(t) = \frac{1}{\sqrt{\tau}} e^{-i\omega_m t} \frac{\sin(\delta\omega t/2)}{\delta\omega t/2}\,. \tag{17}$$

Upon temporal coarse-graining, we combine M old wave packets into one new one, and at the same time the frequency-resolution becomes refined: $\tau' = M\tau$ and $\delta\omega' = \delta\omega/M$. Thus, the new frequency index m' can be thought of as a combination of the old index m and another index $l = 0 \ldots N-1$ that splits the old frequency interval into M pieces. The interval belonging to m' is thus: $\omega \in [(m-1/2)\delta\omega + l\delta\omega', (m-1/2)\delta\omega + (l+1)\delta\omega'[$. The definition of $F'_{m',n'}(\omega)$ on this interval reads like the old one, except for the obvious replacements: $F'_{m',n'}(\omega) = e^{i\omega t'_{n'}}/\sqrt{\delta\omega'}$, with $t'_{n'} \equiv n'\tau' = n'M\tau$. Both the old and the new basis are complete.

We now want to obtain the overlap integrals that relate the old basis to the new one. We find:

$$\langle m', n'|m, n\rangle \equiv \int {F'}^*_{m',n'}(\omega) F_{m,n}(\omega) d\omega = K_{m'}(n - n'M)\,, \tag{18}$$

with

$$K_{m'}(k) = \begin{cases} k = 0: & \frac{1}{\sqrt{M}} \\ k \neq 0: & \sqrt{M}\frac{e^{i\frac{2\pi}{M}k}-1}{2\pi i k}(-1)^k e^{i\frac{2\pi}{M}lk} \end{cases} \tag{19}$$

Note that the overlap K obviously depends on the frequency index m' only via the refinement index l in $m' = (m, l)$, and that $K = 0$ if we were to calculate the overlap for any m' that is not part of the original frequency interval defined by m. The shape of the overlap as a function of the temporal distance $n - n'M$ is that of a sinc function with a decay scale set by M. One can confirm that the overlap matrix elements calculated here are normalized, $\sum_n |K_{m'}(n - n'M)|^2 = 1$.

When we think of the situation with two entangled beams, we imagine each of them is defined by its own fluctuating output field, $\hat{A}_\sigma(t)$, where $\sigma = 1, 2$ denotes the beam. Each of those can be decomposed into the kind of Wannier

basis defined here, and we choose the same filter time τ for each of them. Regarding the frequencies, we want to exploit the fact that in a typical steady-state situation (like in parametric down-conversion or four-wave mixing), it is pairs of frequencies that are entangled. Thus, to each frequency ω_1 of beam 1 belongs an entangled frequency ω_2 of beam 2 (with $\omega_{\text{total}} = \omega_1 + \omega_2$). To simplify the subsequent notation, we want to shift and revert the frequency scale of beam 2 such that the two mutually entangled frequencies are always both denoted by the index m. In other words, while $\omega_1 = m\delta\omega$, we have $\omega_2 = \omega_{\text{total}} - m\delta\omega$. We note that, after going into a rotating frame that makes the Hamiltonian time-independent (as in the main text), we obtain $\omega_{\text{total}} = 0$. In addition, it turns out that due to this matching between opposite frequencies, the basis functions for beam 2 have to be changed accordingly, and the basis transformation for beam 2 is effected by K^* instead of K.

We now want to confirm (as indicated in the main text), that such a coarse-graining does not change the entanglement E between wave packets, provided we are already in the regime of sufficiently large filter time, $\tau \gg \tau_c$. To this end, we just have to show that the correlators between modes do not change upon coarse-graining, i.e. we want to show in particular

$$\left\langle \hat{a}^{(1)}_{m,n} \hat{a}^{(2)}_{m,n} \right\rangle = \left\langle \hat{a}^{'(1)}_{m',n'} \hat{a}^{'(2)}_{m',n'} \right\rangle \tag{20}$$

where the modes on the right-hand side are the temporally coarse-grained ones, and $\omega_{m'}$ lies within the interval defined by m. The precise location of $\omega_{m'}$ within that interval will not matter, since $\delta\omega \ll 1/\tau_c$, so the spectrum of the source is already flat on that scale. In addition, we note that, for the steady-state situation we assume here, neither the left-hand-side nor the right-hand-side of (20) actually depend on the time-point n or n', respectively.

Employing the overlap calculated above, we find:

$$\begin{gathered} \left\langle \hat{a}^{'(1)}_{m',n'} \hat{a}^{'(2)}_{m',n'} \right\rangle = \\ \textstyle\sum_{n_1,n_2} K_{m'}(n_1 - n'M) K^*_{m'}(n_2 - n'M) \left\langle \hat{a}^{(1)}_{m,n_1} \hat{a}^{(2)}_{m,n_2} \right\rangle = \\ \textstyle\sum_n |K_{m'}(n - n'M)|^2 \left\langle \hat{a}^{(1)}_{m,n} \hat{a}^{(2)}_{m,n} \right\rangle = \left\langle \hat{a}^{(1)}_{m,n} \hat{a}^{(2)}_{m,n} \right\rangle \end{gathered} \tag{21}$$

Here we have used that $\hat{a}^{'(1)}_{m',n'} = \sum_{n_1} K_{m'}(n_1 - n'M) \hat{a}^{(1)}_{m,n_1}$ and $\hat{a}^{'(2)}_{m',n'} = \sum_{n_2} K^*_{m'}(n_2 - n'M) \hat{a}^{(2)}_{m,n_2}$. In going to the second line, we exploited the fact that different time slots are already uncorrelated ($\tau \gg \tau_c$). We also used the normalization of K in the last step.

Regarding other correlators, such as $\left\langle \hat{a}^{(1)}_{m,n} \hat{a}^{(2)\dagger}_{m,n} \right\rangle$, we can say the following: For the model discussed in the main text, they can be confirmed to be zero by explicit calculation. For more general models, where however the Hamiltonian can still be brought to a time-independent form by a proper choice of rotating frame, we find that stationarity dictates that $\left\langle \hat{a}^{(1)}(\omega) \left(\hat{a}^{(2)\dagger}\right)(\omega') \right\rangle \propto \delta(\omega + \omega')$, and likewise for all other correlators. In evaluating a correlator of amplitudes in the Wannier-basis, like $\left\langle \hat{a}^{(1)}_{m,n} \hat{a}^{(2)\dagger}_{m,n} \right\rangle$, we are effectively looking at correlators of the type $\left\langle \hat{a}^{(1)}(\omega) \left(\hat{a}^{(2)}(\omega')\right)^\dagger \right\rangle$, with $\omega' \approx -\omega$ [by our definition given above, m enters the frequency ω_2 with an opposite sign]. Since $\left(\hat{a}^{(2)}(\omega')\right)^\dagger = \left(\hat{a}^{(2)\dagger}\right)(-\omega')$, that correlator equals $\left\langle \hat{a}^{(1)}(\omega) \left(\hat{a}^{(2)\dagger}\right)(-\omega') \right\rangle \propto \delta(\omega - \omega')$. By virtue of $\omega' \approx -\omega$, this is zero automatically. (Note that formally we have to exclude the single point $\omega = 0$ in this argument, which would physically equal the incoming laser frequency in the case of four-wave mixing, and the corresponding small frequency slot.) For the correlators involving quantities of the same beam, it is rather correlators of the type $\left\langle \hat{a}^{(1)}_{m,n} \hat{a}^{(1)\dagger}_{m,n} \right\rangle$ that are nonzero, while correlators like $\left\langle \hat{a}^{(1)}_{m,n} \hat{a}^{(1)}_{m,n} \right\rangle$ are zero, and the proof is in analogy to what was shown above. In summary, the entanglement E will go to a well-defined limit as $\tau \to \infty$ ($\tau \gg \tau_c$). (As mentioned above, in taking this limit, we assume the frequency index m is re-adjusted such that the center frequency of the corresponding slot is held fixed at some given ω, thus arriving at $E[\omega]$ in the limit $\tau \to \infty$.) The actual calculation of $E[\omega]$ is discussed below.

C. Hamiltonian and implementation with three coupled optomechanical cells

In this section, we give a derivation of the Hamiltonian (2) and discuss its implementation. We consider three equidistant optical modes with a splitting J coupled to the same mechanical mode $\hat{b}$ with frequency Ω via radiation pressure. One of the optical modes (here called a_0) is driven by an external laser at frequency ω_L. Such a setup in

general can be described by the following Hamiltonian ($\hbar = 1$), where for brevity we do not display the coupling to the dissipative environment:

$$\hat{H} = \sum_{q=\pm,0} \omega_q \hat{a}_q^\dagger \hat{a}_q + \Omega \hat{b}^\dagger \hat{b} - \sum_{q,q'=\pm,0} g_{q',q}^{(0)} \hat{a}_{q'}^\dagger \hat{a}_q (\hat{b} + \hat{b}^\dagger) + \Lambda(\hat{a}_0 e^{i(\omega_L t+\phi)} + \text{h.c.}) \tag{22}$$

Here $\omega_\pm = \omega_0 \pm J$, and $g_{q',q}^{(0)}$ represents the generic (Hermitian) optomechanical coupling matrix. We now assume that the frequency mismatch $\delta \equiv \Omega - J$ is much smaller than the mechanical frequency, i.e., $|\delta| \ll \Omega$ and that the mechanical sidebands are resolved, i.e., $\kappa \ll \Omega$, where κ is the optical damping rate. After transforming to the rotating frame with respect to $\hat{H}_0 = (\omega_L + J)\hat{a}_+^\dagger \hat{a}_+ + (\omega_L - J)\hat{a}_-^\dagger \hat{a}_- + \omega_L \hat{a}_0^\dagger \hat{a}_0 + J\hat{b}^\dagger \hat{b}$, and neglecting rapidly oscillating terms rotating at $\pm J$ by a rotating wave approximation (RWA), we find

$$\hat{H}_{\text{RWA}} = \sum_{q=\pm,0} -\Delta \hat{a}_q^\dagger \hat{a}_q + \delta \hat{b}^\dagger \hat{b} - \{(g_{+,0}^{(0)} \hat{a}_+^\dagger \hat{a}_0 + g_{0,-}^{(0)} \hat{a}_0^\dagger \hat{a}_-)\hat{b} + h.c\} + \Lambda(\hat{a}_0 e^{i\phi} + \hat{a}_0^\dagger e^{-i\phi}) \tag{23}$$

where $\Delta = \omega_L - \omega_0$ is the laser drive detuning. For a sufficiently strong laser drive, we can linearize the dynamics by replacing $\hat{a}_0$ by a complex number $\alpha = \frac{-i\Lambda e^{-i\phi}}{-i\triangle + \kappa/2}$. Thus we find the Hamiltonian (2) as given in the main text

$$\hat{H}_{\text{lin}} = -\triangle(\hat{a}_+^\dagger \hat{a}_+ + \hat{a}_-^\dagger \hat{a}_-) + \delta \hat{b}^\dagger \hat{b} - \frac{g}{2}\{(\hat{a}_+^\dagger + \hat{a}_-)\hat{b} + h.c\}, \tag{24}$$

provided that the couplings to the "+" and "−" mode turn out to be equal, i.e. $g/2 \equiv g_{+,0}^{(0)}\alpha = g_{0,-}^{(0)}\alpha$. Without loss of generality, we assume that g is real-valued. The RWA made above is valid when $|g| \ll \Omega$. It may be unavoidable that there is a small asymmetry in the two optomechanical coupling strengths, but since the entanglement generation involves both transitions simultaneously this does not make a crucial difference (we have confirmed this for the output entanglement which we discuss). A more detailed account on some further aspects of asymmetric optomechanical coupling strengths in the context of this kind of Hamiltonian may be found in [28, 29], where it is pointed out that for the case of intra-cavity entanglement (which is not our concern here) having such an asymmetry can actually be beneficial.

We now turn to deriving the Hamiltonian (22) for a concrete setup consisting of three coupled optomechanical cells. In each of the cells, we assume a standard (local) coupling between photons and phonons. The microscopic Hamiltonian reads ($\hbar = 1$)

$$\hat{H}_{\text{cell}} = \sum_{l=1}^{3} \{\omega_0 \hat{a}_l^\dagger \hat{a}_l + \Omega \hat{b}_l^\dagger \hat{b}_l - g_0 \hat{a}_l^\dagger \hat{a}_l (\hat{b}_l^\dagger + \hat{b}_l)\} - (K_1 \hat{a}_1^\dagger \hat{a}_2 + K_2 \hat{a}_2^\dagger \hat{a}_3 + h.c.) \tag{25}$$

where the index $l = 1, 2, 3$ runs over the three sites. The second term describes photon tunneling between different sites. It can be taken into account by introducing optical normal modes, as defined by $\hat{a}_\pm = (\frac{K_1 \hat{a}_1 + K_2 \hat{a}_3}{\sqrt{K_1^2 + K_2^2}} \mp \hat{a}_2)/\sqrt{2}$, $\hat{a}_0 = \frac{K_2 \hat{a}_1 - K_1 \hat{a}_3}{\sqrt{K_1^2 + K_2^2}}$ with eigenfrequencies $\omega_\pm = \omega_0 \pm \sqrt{K_1^2 + K_2^2}$, ω_0 respectively. In terms of the normal modes, the Hamiltonian can be written as

$$\begin{array}{c} \hat{H}_{\text{cell}} = \sum_{q=\pm,0} \omega_q \hat{a}_q^\dagger \hat{a}_q + \sum_{l=1}^{3} \Omega \hat{b}_l^\dagger \hat{b}_l - \frac{g_0}{2}(\hat{a}_- - \hat{a}_+)^\dagger (\hat{a}_- - \hat{a}_+)(\hat{b}_2^\dagger + \hat{b}_2) \\ -\frac{g_0}{2(K_1^2+K_2^2)}(K_1\hat{a}_+ + K_1\hat{a}_- + \sqrt{2}K_2\hat{a}_0)^\dagger (K_1\hat{a}_+ + K_1\hat{a}_- + \sqrt{2}K_2\hat{a}_0)(\hat{b}_1^\dagger + \hat{b}_1) \\ -\frac{g_0}{2(K_1^2+K_2^2)}(K_2\hat{a}_+ + K_2\hat{a}_- - \sqrt{2}K_1\hat{a}_0)^\dagger (K_2\hat{a}_+ + K_2\hat{a}_- - \sqrt{2}K_1\hat{a}_0)(\hat{b}_3^\dagger + \hat{b}_3) \end{array} \tag{26}$$

This Hamiltonian takes essentially the same form as the Hamiltonian (22) given above. We assume that $\delta = \Omega - \sqrt{K_1^2 + K_2^2} \ll \Omega$ and $\kappa \ll \Omega$, transform to a rotating frame with $\hat{H}_0 = \sum_{q=\pm,0}(\omega_q - \omega_0)\hat{a}_q^\dagger \hat{a}_q + \sum_{l=1}^{3} \sqrt{K_1^2 + K_2^2}\hat{b}_l^\dagger \hat{b}_l$, and apply a RWA to find

$$\hat{H}_{\text{eff}} = \sum_{q=\pm,0} \omega_0 \hat{a}_q^\dagger \hat{a}_q + \sum_{l=1}^{3} \delta \hat{b}_l^\dagger \hat{b}_l - g_0 \frac{K_1 K_2}{K_1^2 + K_2^2}\{(\hat{a}_+^\dagger \hat{a}_0 + \hat{a}_- \hat{a}_0^\dagger)\frac{\hat{b}_1 - \hat{b}_3}{\sqrt{2}} + h.c.\} \tag{27}$$

After adding an external laser drive for the $\hat{a}_0$ mode, moving into a frame rotating with the drive frequency and applying standard linearization, this Hamiltonian is identical in form to the Hamiltonian (2) given in the main text. The relevant mechanical normal mode is given by $\hat{b} = (\hat{b}_1 - \hat{b}_3)/\sqrt{2}$. Note that the design is quite flexible in that it also applies to setups with unbalanced hopping rates $K_1 \neq K_2$ and that, in principle, a mechanical mode coupled only to either the first or the third site would suffice. The $\hat{a}_0$ mode may be driven through an additional channel, provided that the decay rate into this is sufficiently small so as to ensure that the entangled photon pairs dominantly decay into another, outcoupling waveguide.

As pointed out in the main text, a similar configuration of levels may be realized in optomechanical membrane-in-the-middle setups. In such setups, the frequencies of the transverse normal optical modes of the cavity depend on the membrane position and tilt angle [38]. These parameters may be tuned so as to create triplet equidistant optical modes. The frequency separation can be comparable to the frequency of a vibrational mode of the membrane, which could be matched to the optical splitting by applying the optical spring effect [14]. In such a configuration, the (linear) optomechanical coupling strengths are set by the slopes of the optical bands [37]. As pointed out above, even if these turn out to be different, that will not impact our scheme in any important way.

D. Effective optical model

Next, we derive the effective optical model, i.e. the model obtained after integrating out the mechanics. We will discuss how it captures some essential features of the full model. Assuming a large frequency mismatch $\delta \gg \kappa$, Γ, g, $|\Delta|$, and low temperatures, i.e., $\sqrt{n_{\rm th}+1} < g/\kappa$, we can adiabatically eliminate the mechanical mode and the mechanical bath. This can be accomplished by a polaron transformation $\hat{H}_{\rm opt} = e^{\hat{S}}\hat{H}_{\rm lin}e^{-\hat{S}}$ with $\hat{S} = \frac{g}{2(\delta+\triangle)}(\hat{a}_+^\dagger\hat{b} - \hat{a}_+\hat{b}^\dagger) + \frac{g}{2(\delta-\triangle)}(\hat{a}_-\hat{b} - \hat{a}_-^\dagger\hat{b}^\dagger)$. Thus, we find

$$\begin{aligned}\hat{H}_{\rm opt} &= -\triangle(\hat{a}_+^\dagger\hat{a}_+ + \hat{a}_-^\dagger\hat{a}_-) + \delta\hat{b}^\dagger\hat{b} - (\tfrac{g^2}{8(\delta+\triangle)} + \tfrac{g^2}{8(\delta-\triangle)})(\hat{a}_+^\dagger\hat{a}_-^\dagger + \hat{a}_+\hat{a}_-)\\ &\quad -\tfrac{g^2}{4(\delta+\triangle)}\hat{a}_+^\dagger\hat{a}_+ - \tfrac{g^2}{4(\delta-\triangle)}\hat{a}_-^\dagger\hat{a}_- - (\tfrac{g^2}{4(\delta+\triangle)} - \tfrac{g^2}{4(\delta-\triangle)})\hat{b}^\dagger\hat{b}\\ &\approx -\triangle(\hat{a}_+^\dagger\hat{a}_+ + \hat{a}_-^\dagger\hat{a}_-) + \delta\hat{b}^\dagger\hat{b} - \tfrac{g^2}{4\delta}(\hat{a}_+^\dagger\hat{a}_+ + \hat{a}_-^\dagger\hat{a}_- + \hat{a}_+^\dagger\hat{a}_-^\dagger + \hat{a}_+\hat{a}_-).\end{aligned} \tag{28}$$

where, in the last step, we explicitly used that $|\Delta| \ll \delta$. The optical modes are now decoupled from the mechanical mode and we obtain a closed set of quantum Langevin equations for the optical modes

$$\begin{aligned}\dot{\hat{a}}_+ &= i(\triangle + \tfrac{g^2}{4\delta})\hat{a}_+ + i\tfrac{g^2}{4\delta}\hat{a}_-^\dagger - \tfrac{\kappa}{2}\hat{a}_+ - \sqrt{\kappa}\hat{a}_{+,in}(t)\\ \dot{\hat{a}}_+^\dagger &= -i(\triangle + \tfrac{g^2}{4\delta})\hat{a}_+^\dagger - i\tfrac{g^2}{4\delta}\hat{a}_- - \tfrac{\kappa}{2}\hat{a}_+^\dagger - \sqrt{\kappa}\hat{a}_{+,in}^\dagger(t)\\ \dot{\hat{a}}_- &= i(\triangle + \tfrac{g^2}{4\delta})\hat{a}_- + i\tfrac{g^2}{4\delta}\hat{a}_+^\dagger - \tfrac{\kappa}{2}\hat{a}_- - \sqrt{\kappa}\hat{a}_{-,in}(t)\\ \dot{\hat{a}}_-^\dagger &= -i(\triangle + \tfrac{g^2}{4\delta})\hat{a}_-^\dagger - i\tfrac{g^2}{4\delta}\hat{a}_+ - \tfrac{\kappa}{2}\hat{a}_-^\dagger - \sqrt{\kappa}\hat{a}_{-,in}^\dagger(t)\end{aligned} \tag{29}$$

where $\langle\hat{a}_{q,in}\rangle = 0$, $\left\langle\hat{a}_{q,in}^\dagger(t)\hat{a}_{q',in}(t')\right\rangle = 0$, $\left\langle\hat{a}_{q,in}(t)\hat{a}_{q',in}^\dagger(t')\right\rangle = \delta_{qq'}\delta(t-t')$ with $q,q' = \pm$. The output fields are related by $\hat{a}_{\pm,out}(t) = \sqrt{\kappa}\hat{a}_\pm(t) + \hat{a}_{\pm,in}(t)$. For notational convenience, we introduce the operator vectors $A = (\ \hat{a}_+\ \ \hat{a}_+^\dagger\ \ \hat{a}_-\ \ \hat{a}_-^\dagger\ )^T$ and $A_{in} = (\ \hat{a}_{+,in}\ \ \hat{a}_{+,in}^\dagger\ \ \hat{a}_{-,in}\ \ \hat{a}_{-,in}^\dagger\ )^T$. The quantum Langevin equations can be cast in the following compact form

$$\dot{A} = MA - \sqrt{\kappa}A_{in} \tag{30}$$

where

$$M = \begin{pmatrix} i(\triangle + \frac{g^2}{4\delta}) - \frac{\kappa}{2} & 0 & 0 & i\frac{g^2}{4\delta} \\ 0 & -i(\triangle + \frac{g^2}{4\delta}) - \frac{\kappa}{2} & -i\frac{g^2}{4\delta} & 0 \\ 0 & i\frac{g^2}{4\delta} & i(\triangle + \frac{g^2}{4\delta}) - \frac{\kappa}{2} & 0 \\ -i\frac{g^2}{4\delta} & 0 & 0 & -i(\triangle + \frac{g^2}{4\delta}) - \frac{\kappa}{2} \end{pmatrix}.$$

The system is stable only if all eigenvalues of M have non-positive real parts. The boundary of stability is located where one of the real parts becomes zero, i.e., $-\frac{\kappa}{2} + \sqrt{-(\frac{g^2}{2\delta} + \triangle)\triangle} = 0$, or equivalently when $(\Delta + g^2/(2\delta))\Delta + \kappa^2/4 = 0$.

This corresponds to the dashed line in Fig. 4a. Note that the lower quadrants of the stability diagram are essentially identical due to inversion symmetry with respect to the point $\delta = \Delta = 0$.

We can solve the quantum Langevin equations in Fourier space. We define the Fourier-transformed operators by $\hat{a}_+(\omega) = \int_{-\infty}^{+\infty} \hat{a}_+(t)e^{i\omega t}dt$, $\hat{a}_+^\dagger(-\omega) \equiv \int_{-\infty}^{+\infty} \hat{a}_+^\dagger(t)e^{i\omega t}dt = (\hat{a}_+^\dagger)(\omega)$. In the frequency domain, the input noise correlation reads $\left\langle \hat{a}_{q,in}(\omega)\hat{a}^\dagger_{q',in}(-\omega')\right\rangle = 2\pi\delta_{qq'}\delta(\omega+\omega')$. For convenience, we define the vectors $A_{in/out}(\omega) = (\ \hat{a}_{+,in/out}(\omega)\ \ \hat{a}^\dagger_{+,in/out}(-\omega)\ \ \hat{a}_{-,in/out}(\omega)\ \ \hat{a}^\dagger_{-,in/out}(-\omega)\ )^T$. The solution of the Langevin equation can be written as $A_{out}(\omega) = S(\omega)A_{in}(\omega)$ with the scattering matrix

$$S(\omega) = \frac{\kappa}{M_{14}^2 + (M_{11}+i\omega)(M_{22}+i\omega)} \begin{pmatrix} M_{22}+i\omega & 0 & 0 & -M_{14} \\ 0 & M_{11}+i\omega & M_{14} & 0 \\ 0 & -M_{14} & M_{22}+i\omega & 0 \\ M_{14} & 0 & 0 & M_{11}+i\omega \end{pmatrix} + I \tag{31}$$

where I is the 4×4 identity matrix. The input noise correlations $B_{in}(\omega,\omega') = \left\langle A_{in}(\omega)\otimes A_{in}^{\mathrm{T}}(\omega')\right\rangle$ are scattered into $B_{out}(\omega,\omega') = \left\langle A_{out}(\omega)\otimes A_{out}^{\mathrm{T}}(\omega')\right\rangle = S(\omega)B_{in}(\omega,\omega')S^T(\omega')$.

In the effective optical model, photons are only created in pairs. The pair creation rate Γ_{pairs} is equal to the intensity (photons/sec) in any of the two output streams. Due to the choice of normalization in the input-output formalism, this is given by:

$$\begin{aligned} \left\langle \hat{a}^\dagger_{\pm,out}\hat{a}_{\pm,out}\right\rangle &= (\tfrac{1}{2\pi})^2 \int_{-\infty}^{+\infty} d\omega \int_{-\infty}^{+\infty} d\omega' \left\langle \hat{a}^\dagger_{\pm,out}(-\omega)\hat{a}_{\pm,out}(\omega')\right\rangle \\ &= \tfrac{(g^2/4\delta)^2\kappa/2}{(\kappa/2)^2+(\triangle+\frac{g^2}{2\delta})\triangle} \end{aligned} \tag{32}$$

This result shows that, depending on the sign of $(\triangle + \frac{g^2}{2\delta})\triangle$, we get an enhanced or decreased photon pair creation rate compared with $\triangle = 0$. In addition, since the denominator vanishes at the boundary of stability, the photon pair creation rate diverges there.

E. Calculation of $E[\omega]$

Here, we review the definition of the logarithmic negativity and apply it to quantify the entanglement of the filtered optical output fields, first for the effective optical model introduced above, and then for the full model. By applying narrow frequency filters, we select only single-frequency components of each of the optical output fields. By energy conservation, correlations only occur between the ω-component of one of the fields (say $\hat{a}_{+,out}$) and the $-\omega$-component of the other ($\hat{a}_{-,out}$). The field operators for these two single-frequency output fields are obtained as $\hat{a}_{+,\omega}(t) = \int_{-\infty}^t f(t-s)\hat{a}_{+,out}(s)ds$, $\hat{a}_{-,-\omega}(t) = \int_{-\infty}^t g(t-s)\hat{a}_{-,out}(s)ds$. For convenience, we now will choose Lorentzian filter functions $f(t) = \sqrt{\frac{2}{\tau}}\theta(t)e^{-(\frac{1}{\tau}-i\omega)t}$, $g(t) = \sqrt{\frac{2}{\tau}}\theta(t)e^{-(\frac{1}{\tau}+i\omega)t}$ with $\theta(t)$ the Heaviside step function, as opposed to the Wannier basis used in the main text. In the limit of small bandwidth $1/\tau \to 0$, which is the only one we discuss, however, both the basis function probability densities reduce to Dirac δ-functions, and the results will co-incide.

We can use the logarithmic negativity [9] to characterize the entanglement for the output light beams [21]. In order to evaluate it, we define the vector $u = (\ \hat{x}_{+,\omega}(t)\ \ \hat{p}_{+,\omega}(t)\ \ \hat{x}_{-,-\omega}(t)\ \ \hat{p}_{-,-\omega}(t)\ )^T$ with $\hat{x}_j(t) = \frac{1}{\sqrt{2}}(\hat{a}_j(t)+\hat{a}_j^\dagger(t))$, $\hat{p}_j(t) = \frac{1}{\sqrt{2}i}(\hat{a}_j(t)-\hat{a}_j^\dagger(t))$ ($j = +,\omega$ or $j = -,-\omega$). The entanglement is determined by the covariance matrix V with matrix elements $V_{ij} = \frac{1}{2}\left\langle u_iu_j + u_ju_i\right\rangle$, where the operators involved in this product are all taken at equal times. Inserting the stationary solution, we find

$$V = \begin{pmatrix} n_+ & 0 & \mathrm{Re}(\xi) & \mathrm{Im}(\xi) \\ 0 & n_+ & \mathrm{Im}(\xi) & -\mathrm{Re}(\xi) \\ \mathrm{Re}(\xi) & \mathrm{Im}(\xi) & n_- & 0 \\ \mathrm{Im}(\xi) & -\mathrm{Re}(\xi) & 0 & n_- \end{pmatrix}, \tag{33}$$

where

$$n_+ = \int_{-\infty}^{+\infty} e^{-i\omega t} \left\langle \hat{a}^\dagger_{+,\mathrm{out}}(t)\hat{a}_{+,\mathrm{out}}(0)\right\rangle \, dt + 1/2 = |S_{14}(\omega)|^2 + 1/2\,,$$

$$n_- = \int_{-\infty}^{+\infty} e^{i\omega t} \left\langle \hat{a}^\dagger_{-,\mathrm{out}}(t)\hat{a}_{-,\mathrm{out}}(0)\right\rangle \, dt + 1/2 = |S_{14}(\omega)|^2 + 1/2\,,$$

and

$$\xi = \int_{-\infty}^{+\infty} e^{i\omega t} \left\langle \hat{a}_{+,\mathrm{out}}(t)\hat{a}_{-,\mathrm{out}}(0)\right\rangle \, dt = S_{11}(\omega)S_{14}(-\omega)\,.$$

The logarithmic negativity is defined as $E = max[0, -ln(2\eta_-)]$ with $\eta_- = \frac{n_+ + n_-}{2} - \sqrt{(\frac{n_+ - n_-}{2})^2 + |\xi|^2}$ being the smaller symplectic eigenvalue of the partial transpose of matrix V. Choosing $\omega = 0$, we plot $E[\omega = 0]$ as a function of $\triangle/\kappa$ in Fig. 4b.

To obtain the spectral density of entanglement in the full model, we solve the following system of quantum Langevin equations, which derive directly from the model Hamiltonian (main text), and where dissipation and fluctuations have been taken into account using the usual input-output formalism:

$$\begin{array}{c}
\dot{\hat{a}}_+ = i\triangle\hat{a}_+ + i\frac{g}{2}\hat{b} - \frac{\kappa}{2}\hat{a}_+ - \sqrt{\kappa}\hat{a}_{+,in}(t) \\
\dot{\hat{a}}^\dagger_+ = -i\triangle\hat{a}^\dagger_+ - i\frac{g}{2}\hat{b}^\dagger - \frac{\kappa}{2}\hat{a}^\dagger_+ - \sqrt{\kappa}\hat{a}^\dagger_{+,in}(t) \\
\dot{\hat{a}}_- = i\triangle\hat{a}_- + i\frac{g}{2}\hat{b}^\dagger - \frac{\kappa}{2}\hat{a}_- - \sqrt{\kappa}\hat{a}_{-,in}(t) \\
\dot{\hat{a}}^\dagger_- = -i\triangle\hat{a}^\dagger_- - i\frac{g}{2}\hat{b} - \frac{\kappa}{2}\hat{a}^\dagger_- - \sqrt{\kappa}\hat{a}^\dagger_{-,in}(t) \\
\dot{\hat{b}} = -i\delta\hat{b} + i\frac{g}{2}(\hat{a}_+ + \hat{a}^\dagger_-) - \frac{\Gamma}{2}\hat{b} - \sqrt{\Gamma}\hat{b}_{in}(t) \\
\dot{\hat{b}}^\dagger = i\delta\hat{b}^\dagger - i\frac{g}{2}(\hat{a}_- + \hat{a}^\dagger_+) - \frac{\Gamma}{2}\hat{b}^\dagger - \sqrt{\Gamma}\hat{b}^\dagger_{in}(t)
\end{array} \tag{34}$$

where, in addition, we have $\left\langle \hat{b}_{in}\right\rangle = 0$, $\left\langle \hat{b}^\dagger_{in}(t)\hat{b}_{in}(t')\right\rangle = n_{\mathrm{th}}\delta(t-t')$, $\left\langle \hat{b}_{in}(t)\hat{b}^\dagger_{in}(t')\right\rangle = (n_{\mathrm{th}}+1)\delta(t-t')$, with $n_{\mathrm{th}} = (\exp(\hbar\Omega/(k_{\mathrm{B}}T)) - 1)^{-1}$. For the logarithmic negativity, we need to evaluate the same optical correlations as above. The results are analytical, but too complicated to be reported here. Simpler analytic results can be found for $\delta = \Delta = 0$. In this case we find $\eta_-(\omega, \delta, \triangle = 0) = 4\mathcal{C}(\mathcal{C} + n_{\mathrm{th}} + \frac{1}{2}) + \frac{1}{2} - 2\mathcal{C}\sqrt{1 + 4(\mathcal{C} + n_{\mathrm{th}} + \frac{1}{2})^2}$ with the cooperativity $\mathcal{C} = \frac{g^2}{\Gamma\kappa}$. The entanglement $E[\omega, \delta, \triangle = 0]$ is only determined by $\mathcal{C}$ and n_{th} as given in the main text.

F. Comparison to two- and three-mode schemes

Finally, we compare the efficiency of our four-mode setup (3 optical, 1 vibrational) to two- and three-mode schemes that have been discussed previously. We show that the four-mode setup is more efficient than either of these schemes.

For a two-mode setup (1 optical, 1 vibrational) and with a resonant laser drive (detuning $\Delta = 0$), the Hamiltonian is given by $\hat{H} = \Omega\hat{b}^\dagger b - g(\hat{a} + \hat{a}^\dagger)(\hat{b} + \hat{b}^\dagger)$, where $\hat{a}$ is an optical and $\hat{b}$ is a mechanical mode (see [14] and [21] for the case of drive at the red mechanical sideband). The filtered correlations that quantify the entanglement between the Stokes and anti-Stokes mechanical sidebands are then given by

$$\begin{array}{r}
n_+ = \frac{\kappa^2 g^4}{(\Omega^2 + (\kappa/2)^2)^2(\Gamma/2)^2} + \frac{2n_{\mathrm{th}}\kappa g^2}{(\Omega^2 + (\kappa/2)^2)(\Gamma/2)} + \frac{1}{2} \\
n_- = \frac{\kappa^2 g^4}{(\Omega^2 + (\kappa/2)^2)^2(\Gamma/2)^2} + \frac{2(n_{\mathrm{th}}+1)\kappa g^2}{(\Omega^2 + (\kappa/2)^2)(\Gamma/2)} + \frac{1}{2} \\
\xi = -\frac{\kappa^2 g^4}{(\Omega^2 + (\kappa/2)^2)^2(\Gamma/2)^2} - \frac{(2n_{\mathrm{th}}+1)\kappa g^2}{(\Omega^2 + (\kappa/2)^2)(\Gamma/2)}
\end{array} \tag{35}$$

where we have assumed that $\Omega \gg \Gamma$. For our model, with resonant drive $\Delta = 0$, we find

$$\begin{array}{r}
n_+ = \frac{\kappa\Gamma n_{\mathrm{th}}(g/2)^2}{[(-\omega+\delta)^2 + (\Gamma/2)^2](\omega^2 + (\kappa/2)^2)} + \frac{\kappa^2(g/2)^4}{[(-\omega+\delta)^2 + (\Gamma/2)^2](\omega^2 + (\kappa/2)^2)^2} + \frac{1}{2} \\
n_- = \frac{\kappa\Gamma(n_{\mathrm{th}}+1)(g/2)^2}{[(-\omega+\delta)^2 + (\Gamma/2)^2](\omega^2 + (\kappa/2)^2)} + \frac{\kappa^2(g/2)^4}{[(-\omega+\delta)^2 + (\Gamma/2)^2](\omega^2 + (\kappa/2)^2)^2} + \frac{1}{2} \\
\xi = -\frac{\kappa^2(g/2)^4}{[(-\omega+\delta)^2 + (\Gamma/2)^2](\omega^2 + (\kappa/2)^2)^2} + \frac{-\kappa\Gamma(n_{\mathrm{th}}+1/2)(g/2)^2 + i(-\omega+\delta)\kappa(g/2)^2}{[(-\omega+\delta)^2 + (\Gamma/2)^2](\omega^2 + (\kappa/2)^2)}
\end{array} \tag{36}$$

In order to evaluate the entanglement between the Stokes and anti-Stokes sidebands, we set $\omega = \delta$. This yields

$$\begin{aligned} n_+ &= \frac{2\kappa n_{\rm th}(g/2)^2}{(\Gamma/2)(\delta^2+(\kappa/2)^2)} + \frac{\kappa^2(g/2)^4}{(\Gamma/2)^2(\delta^2+(\kappa/2)^2)^2} + \frac{1}{2} \\ n_- &= \frac{2\kappa(n_{\rm th}+1)(g/2)^2}{(\Gamma/2)(\delta^2+(\kappa/2)^2)} + \frac{\kappa^2(g/2)^4}{(\Gamma/2)^2(\delta^2+(\kappa/2)^2)^2} + \frac{1}{2} \\ \xi &= -\frac{\kappa^2(g/2)^4}{(\Gamma/2)^2(\delta^2+(\kappa/2)^2)^2} - \frac{\kappa(2n_{\rm th}+1)(g/2)^2}{(\Gamma/2)(\delta^2+(\kappa/2)^2)} \end{aligned} \tag{37}$$

By comparing the coherent parts of n_+ and n_- (the terms that do not depend on $n_{\rm th}$ and are useful for optical entanglement), we find that, in our setup, the photon pair creation rate is enhanced by a factor $\sim \frac{\Omega^4}{(\delta^2+(\kappa/2)^2)^2}$.

The main benefit of our setup in comparison to three-mode schemes, which involve one mechanical and two optical modes, is that the laser drive is resonant so that, for a fixed drive strength Λ, the effective optomechanical coupling strength is much larger. By contrast, in a three-mode setup, the laser drives are off-resonant by $\pm\Omega$ so that $|\alpha| = \frac{\Lambda}{\sqrt{\Omega^2+(\kappa/2)^2}}$, whereas in our setup, with $\Delta = 0$, we have $|\alpha| = \frac{2\Lambda}{\kappa}$. Since the intensity of entangled photons scales with g^4 and $g \propto \alpha g_0$, this leads to an enhancement of $\sim (\frac{2\Omega}{\kappa})^4$ of the photon pair creation rate.

[1] A. Einstein, B. Podolsky and N. Rosen, *Phys. Rev.* **47**, 777 (1935).
[2] L. M. Duan, G. Giedke, J. I. Cirac and P. Zoller, *Phys. Rev. Lett.* **84**, 2722 (2000).
[3] W. P. Bowen, R. Schnabel, P. K. Lam and T. C. Ralph, *Phys. Rev. Lett.* **90**, 043601 (2003).
[4] J. Eisert and M.B. Plenio, *Int. J. Quant. Inf.* **1**, 479 (2003).
[5] S. L. Braunstein and P. van Loock, *Rev. Mod. Phys.* **77**, 513 (2005).
[6] M. D. Reid, P. D. Drummond, W. P. Bowen, E. G. Cavalcanti, P. K. Lam, H. A. Bachor, U. L. Andersen and G. Leuchs, *Rev. Mod. Phys.* **81**, 1727 (2009).
[7] U. L. Andersen, G. Leuchs and C. Silberhorn, *Laser & Photonics Reviews* **4**, 337 (2010).
[8] M. Schmidt, M. Ludwig and F. Marquardt, *New J. Phys.* **14**, 125005 (2012).
[9] G. Vidal and R. F. Werner, *Phys. Rev. A* **65**, 032314 (2002); M. B. Plenio, *Phys. Rev. Lett.* **95**, 090503 (2005).
[10] E. Flurin, N. Roch, F. Mallet, M. H. Devoret and B. Huard, *Phys. Rev. Lett.* **109**, 183901 (2012).
[11] C. Eichler, D. Bozyigit, C. Lang, M. Baur, L. Steffen, J. M. Fink, S. Filipp and A. Wallraff, *Phys. Rev. Lett.* **107**, 113601 (2011).
[12] Z. Y. Ou, S. F. Pereira, H. J. Kimble and K. C. Peng, *Phys. Rev. Lett.* **68**, 3663 (1992).
[13] J. U. Fürst, D. V. Strekalov, D. Elser, A. Aiello, U. L. Andersen, Ch. Marquardt and G. Leuchs, *Phys. Rev. Lett.* **106**, 113901 (2011).
[14] M. Aspelmeyer, T. J. Kippenberg and F. Marquardt, *Rev. Mod. Phys.* **86**, 1391 (2014).
[15] K. Hammerer, C. Genes, D. Vitali, P. Tombesi, G. Milburn, C. Simon and D. Bouwmeester, in 'Cavity Optomechanics: Nano- and Micromechanical Resonators Interacting with Light', edited by M. Aspelmeyer, T. J. Kippenberg, F. Marquardt (Springer-Verlag, Berlin Heidelberg, 2014).
[16] D. Vitali, S. Gigan, A. Ferreira, H. R. Böhm, P. Tombesi, A. Guerreiro, V. Vedral, A. Zeilinger and M. Aspelmeyer, *Phys. Rev. Lett.* **98**, 030405 (2007).
[17] A. Mari and J. Eisert, *Phys. Rev. Lett.* **103**, 213603 (2009).
[18] U. Akram, W. Munro, K. Nemoto and G. J. Milburn, *Phys. Rev. A* **86**, 042306 (2012).
[19] S. G. Hofer, W. Wieczorek, M. Aspelmeyer and K. Hammerer, *Phys. Rev. A*, **84**, 052327 (2011).
[20] J. Zhang, K. Peng and S. L. Braunstein, *Phys. Rev. A* **68**, 013808 (2003).
[21] C. Genes, A. Mari, P. Tombesi and D. Vitali, *Phys. Rev. A* **78**, 032316 (2008).
[22] C. Genes, A. Mari, D. Vitali and P. Tombesi, *Adv. At. Mol. Opt. Phys.* **57**, 33 (2009).
[23] C. Wipf, T. Corbitt, Y. Chen and N. Mavalvala, *New J. Phys.* **10**, 095017 (2008).
[24] M. Paternostro, D. Vitali, S. Gigan, M. S. Kim, C. Brukner, J. Eisert and M. Aspelmeyer, *Phys. Rev. Lett.* **99**, 250401 (2007).
[25] Zhang-qi Yin and Y.-J. Han, *Phys. Rev. A* **79**, 024301 (2009).
[26] Sh. Barzanjeh, M. Abdi, G. J. Milburn, P. Tombesi and D. Vitali, *Phys. Rev. Lett.* **109**, 130503 (2012).
[27] S. Barzanjeh, S. Pirandola and C. Weedbrook, *Phys. Rev. A* **88**, 042331 (2013).
[28] Y. D. Wang and A. A. Clerk, *Phys. Rev. Lett.* **110**, 253601 (2013).
[29] L. Tian, *Phys. Rev. Lett.* **110**, 233602 (2013).
[30] Y.-D. Wang, S. Chesi and A. A. Clerk, *Phys. Rev. A* **91**, 013807 (2015).
[31] M. C. Kuzyk, S. J. van Enk and H. Wang, *Phys. Rev. A* **88**, 062341 (2013).
[32] T. A. Palomaki, J. D. Teufel, R. W. Simmonds and K. W. Lehnert, *Science* **342**, 710 (2013).
[33] K. Audenaert, J. Eisert, and M. B. Plenio, *Phys. Rev. A* **66**, 042327 (2002).
[34] Note that the phrase "entanglement spectrum" has already a different meaning, which is why we prefer to use "spectral density of entanglement".
[35] A. A. Clerk, M. H. Devoret, S. M. Girvin, Florian Marquardt, and R. J. Schoelkopf, *Rev. Mod. Phys.* **82**, 1155 (2010).

[36] J. D. Thompson, B. M. Zwickl, A. M. Jayich, F. Marquardt, S. M. Girvin and J. G. E. Harris, *Nature* **452**, 72 (2008).
[37] J. C. Sankey, C. Yang, B. M. Zwickl, A. M. Jayich and J. G. E. Harris, *Nat. Phys.* **6**, 707 (2010).
[38] J. C. Sankey, A. M. Jayich, B. M. Zwickl, C. Yang and J. G. E. Harris, in *Proceedings of the XXI International Conference on Atomic Physics*, edited by R. Cote, P. L. Gould, and M. Rozman, (World Scientific, Singapore, 2009).
[39] M. Eichenfield, J. Chan, R. M. Camacho, K. J. Vahala and O. Painter, *Nature* **462**, 78 (2009) .
[40] A. H. Safavi-Naeini and O. Painter, *Opt. Express* **18**, 14926 (2010) .
[41] C. W. Gardiner and M. J. Collett, *Phys. Rev. A* **31**, 3761 (1985) .
[42] M. J. Collett and C. W. Gardiner, *Phys. Rev. A* **30**, 1386 (1984).
[43] D. F. Walls and G. J. Milburn, Quantum Optics 2nd edition (Springer-Verlag, Berlin-Heidelberg, 2008).
[44] J. Gea-Banacloche, N. Lu, L. M. Pedrotti, S. Prasad, M. O. Scully and K. Wódkiewicz, *Phys. Rev. A* **41**, 369 (1990).